Wind Estimation based on Flight Dynamics of Unmanned Aerial Vehicle: Influencing Variables and Its Environmental Application

Dukun Chen[1,2], Weifeng Su[1], Shaojie Jiang[1,3], Honglong Yang[5], Chunsheng Zhang[5], Shutong Jiang[6], Dongyang Chang[6], Yuxin Liang[1], Hao Wang[7], Xin Yang[1], Tzung-May Fu[1], Zhenzhong Zeng[1], Lei Zhu[1], Huizhong Shen[1], Chen Wang[1], Jianhuai Ye[1,2,4,*]

[1]State Key Laboratory of Soil Pollution Prevention and Remediation for Soil Security, Southern University of Science and Technology, Shenzhen 518055, China

[2]Shenzhen Key Laboratory of Precision Measurement and Early Warning Technology for Urban Environmental Health Risks, School of Environmental Science and Engineering, Southern University of Science and Technology, Shenzhen 518055, China

[3]Jiangsu Key Laboratory of Atmospheric Environment Monitoring and Pollution Control, School of Environmental Science and Engineering, Nanjing University of Information Science and Technology, Nanjing, 210000, China

[4]Guangdong Provincial Observation and Research Station for Coastal Atmosphere and Climate of the Greater Bay Area, Shenzhen, 518055, China

[5]Shenzhen National Climate Observatory, Meteorological Bureau of Shenzhen Municipality, Shenzhen 518040, China

[6]Soarability Pte. Ltd., Singapore 409051, Singapore

[7]Shenzhen Key Laboratory for Air Vehicle and Gust Simulation, School of Mechanics and Aerospace Engineering, Southern University of Science and Technology, Shenzhen 518055, China

Correspondence to: Jianhuai Ye (yejh@sustech.edu.cn)

Abstract. Accurate measurement of wind speed and direction is critical for atmospheric and environmental sciences, but achieving high spatiotemporal resolution with operational flexibility remains challenging. This study develops and validates an approach for estimating wind fields based on the flight dynamics of an unmanned aerial vehicle (UAV). Through controlled wind wall experiments, we established a relationship between UAV attitude (inclination angle) and wind speed, demonstrating a rapid response time of less than one second. This relationship is not universal and varies significantly with relative wind direction and payload configuration due to the flight control system and asymmetric airframe of the UAV deployed, demonstrating the necessity of platform-specific calibration for practical application. The performance of this attitude-based method was compared against measurements from a calibrated onboard ultrasonic anemometer. While the sensor-based method achieved good accuracy during hovering and low-speed vertical flights, its performance degraded at higher vertical speeds (>2 m/s) due to rotor-induced airflow interference. In contrast, the attitude-based method maintained robust accuracy across all flight regimes. Furthermore, we developed a machine learning model that incorporated attitude data, flight dynamics, and air pressure to provide high-fidelity wind estimates ($R^2 > 0.90$), which was successfully applied to both hovering and vertical profiling during field campaigns. Validation against a meteorological tower and deployment in coastal observations confirmed the reliability of the machine-learning method. This work presents a sensor-free, computationally efficient framework for obtaining high-resolution wind data. By addressing the critical, platform-specific factors affecting estimation accuracy, our approach enhances the applicability of UAVs for advanced environmental monitoring, atmospheric research, and safety assessments in the emerging low-altitude economy.
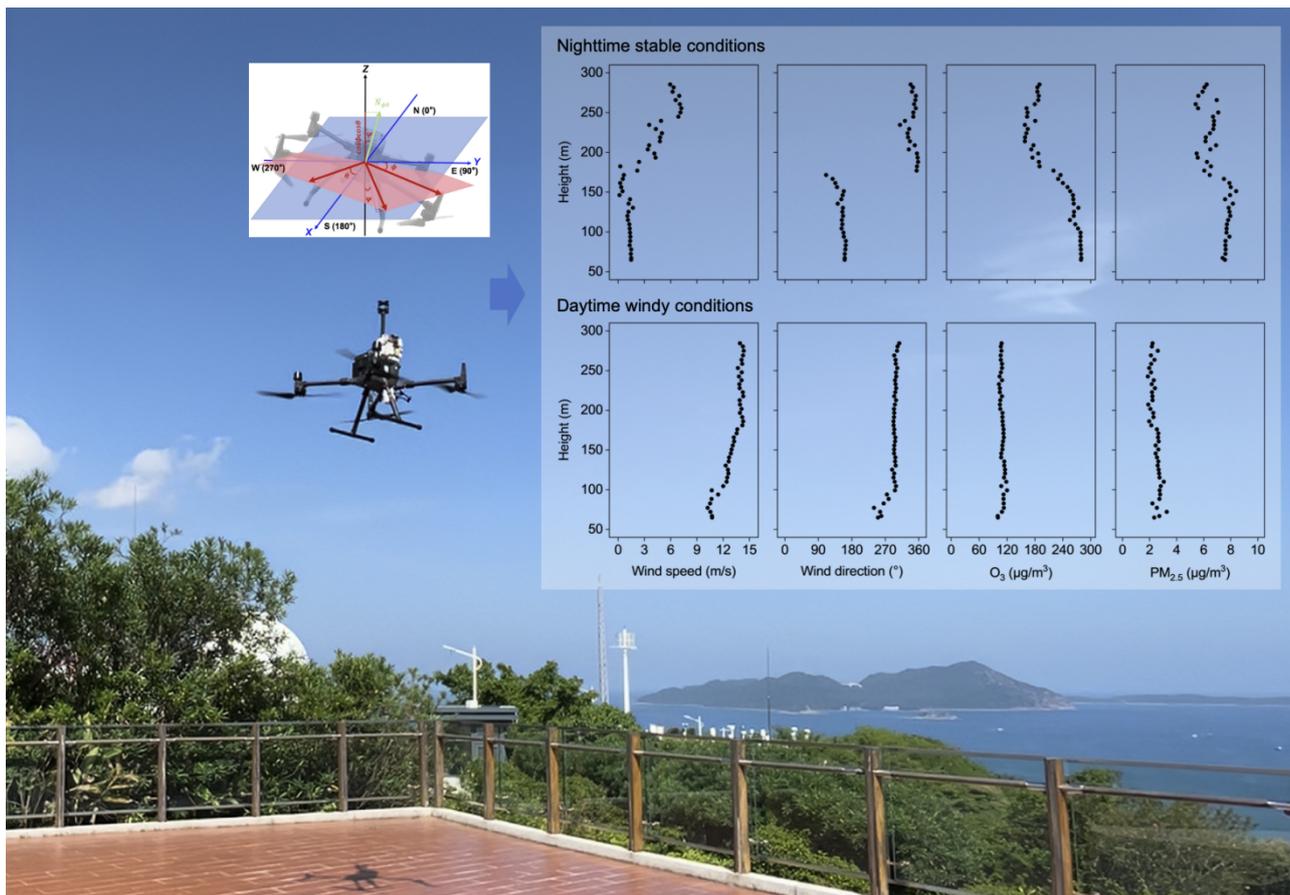
1. Introduction

Wind speed and direction are among the most fundamental and critical observational elements in atmospheric and environmental sciences (Yang et al., 2017; Horton et al., 2014; Wang and Chen, 2016; Guo et al., 2016; Yang et al., 2016). Accurate measurement of these parameters is vital across fields such as pollution monitoring, weather forecasting, and urban planning (Curbelo and Rypina, 2023; Yang et al., 2025a; Salmabadi et al., 2020; Alizadeh et al., 2022; Tominaga and Shirzadi, 2021). Wind direction determines the transport trajectories of air pollutants, while wind speed affects their dispersion and dilution rates. For instance, real-time wind data coupled with atmospheric dispersion models can predict smoke plume trajectories from wildfires (Curbelo and Rypina, 2023) or the spread of toxic gases from industrial emissions (Yang et al., 2025a), enabling authorities to issue timely health advisories and coordinate emergency responses. In regard to weather forecasting, wind directly influences the development and evolution of weather systems and serves as an essential parameter for numerical weather prediction models (Salmabadi et al., 2020; Alizadeh et al., 2022). In the context of urban planning and building design, wind patterns significantly influence thermal distribution within urban environments. Wind-driven cross-ventilation and street canyon airflow dynamics play crucial roles in regulating local microclimates (Tominaga and Shirzadi, 2021). Strategic urban design incorporating prevailing wind speed and direction can optimize ventilation corridors and building layouts to enhance airflow, mitigate heat accumulation, and improve pollutant dispersion.

Achieving high spatiotemporal-resolution wind measurements poses a significant challenge. Traditionally, wind speed and direction have been measured by techniques such as cup and vane anemometers, laser doppler anemometers, ultrasonic anemometers, and remote sensing (such as satellite and radar). However, these methods vary significantly in their accuracy, cost, and environmental suitability. For example, mechanical anemometers (e.g., cup and vane types) are widely employed in meteorological and wind energy applications due to their structural simplicity and cost-effectiveness, but their performance is limited by factors such as turbulence sensitivity, low-altitude measurement constraints, dynamic response lag due to inherent mechanical inertia, and reduced accuracy in low air-density environments (Pindado et al., 2014; Alfonso-Corcuera et al., 2022). In contrast, optical-based systems demonstrate micro-scale resolution and multi-directional capability, but require stringent deployment conditions due to high costs and light propagation sensitivity (Lee, 2003; Diasinos et al., 2013; Knöller et al., 2024). Ultrasonic anemometers achieve high precision through non-mechanical design and wide measurement range, though they are vulnerable to temperature and humidity variations and have multipath interference (Han et al., 2008; Richiardone et al., 2012; Gaeta Lopes et al., 2017; Shan et al., 2023). Finally, remote sensing technologies such as satellite observations provide global coverage for large-scale circulation studies but suffer from fine spatiotemporal resolution limitations (Feng et al., 2023; Hauser et al., 2023).

In recent years, unmanned aerial vehicles (UAVs) have demonstrated broad application potential in atmospheric and environmental sciences due to their unique advantages, such as low cost, flexible deployment, and the ability to obtain high-resolution three-dimensional pollution datasets (Batista et al., 2019; Zhao et al., 2021; Ye et al., 2021; Asher et al., 2021; Ye

et al., 2022; Achermann et al., 2024; Li et al., 2025). Among UAVs, copter-type platforms are emerging as especially effective for wind field measurement and monitoring (Neumann and Bartholmai, 2015; González-Rocha et al., 2023; Ahmed et al., 2024). Their ability to hover and perform vertical profiling at fixed locations provides a key advantage over fixed-wing UAVs for high-resolution measurements (Li et al., 2025). This study, therefore, focuses on copter-type UAVs unless otherwise mentioned.

Current UAV-based wind estimation mainly encompasses three technical paradigms. The first approach involves direct measurement through onboard sensors like anemometers. However, this method often faces challenges such as signal interference from rotor-induced turbulence and measurement inaccuracy during UAV tilt maneuvers (Liu et al., 2023; Yang et al., 2025b). The second approach utilizes mechanical model-based estimation, reconstructing wind fields by analyzing UAV flight attitude (such as roll and pitch angles). Representative models include the dynamic particle model, kinematic particle model, and rigid body model (Sikkel et al., 2016; González-Rocha et al., 2019, 2023; Ahmed et al., 2024). While these methods provide accurate wind estimates, they are computationally expensive and struggle to precisely model UAV-wind interactions under complex atmospheric conditions. The third paradigm employs data-driven analysis by established relationships between wind characteristics and UAV flight attitude (Neumann and Bartholmai, 2015; Brosy et al., 2017; Palomaki et al., 2017). This method offers distinct advantages, such as eliminating the need for additional sensors, which reduces payload weight and power consumption, simplifies system integration, and enhances flight endurance and maneuverability. However, lacking a physical-mechanical representation, it depends on pre-flight training data from controlled wind tests and real-world calibration against reference instruments.

From the perspective of system integration simplicity, cost-effectiveness, and environmental adaptability, UAV attitude-based wind estimation methods show strong potential for modern unmanned systems. While previous studies have explored such methods, critical factors affecting estimation accuracy, including payload characteristics (size and placement), rotor-induced aerodynamic effects, and the relative wind direction with respect to UAV orientation (especially for asymmetric airframes), remain understudied. These parameters significantly influence UAV attitude dynamics and, consequently, the reliability of wind estimates. Moreover, existing studies predominantly focus on wind estimation during hovering or horizontal flights, paying insufficient attention to vertical wind variability. This gap is particularly significant for research on air pollutant dispersion and boundary layer dynamics. Furthermore, the lack of comparative validation under real-world meteorological conditions constrains the practical deployment of literature results.

To address these challenges, this study combines laboratory wind wall experiments with field campaigns (Figures 1A-1C), aiming to systematically examine how the above factors affect attitude-based wind estimation and to evaluate the feasibility of using this approach for real-world vertical wind profiling. Unless otherwise noted, "wind estimation" in this study refers to the estimation of the horizontal wind components. The results are expected to improve the accuracy, robustness, and operational relevance of UAV-based wind sensing for atmospheric research and environmental monitoring.

2. Methods

2.1 UAV platform

A quadcopter UAV (DJI M300 RTK) was used in this study. It has dimensions of 810 × 670 × 430 mm³ (L × W × H) when unfolded. The weight of the UAV is 6.3 kg with batteries. The maximum flight weight of the payload is 2.7 kg, and the maximum flight time is 55 min. The maximum ascent and descent speeds of the UAV reach 6 m/s and 5 m/s, respectively. The hovering accuracy ranges from 0.1 to 0.5 m, and the maximum tolerable wind speed is 12 m/s. The UAV is equipped with an inertial measurement unit and a GPS positioning system, which can output the attitude and flight dynamics information required for wind estimation.

2.2 Wind measurement and estimation

UAV-based wind measurements and estimations were conducted at the Laboratory for Air Vehicle and Gust Simulation facility at Southern University of Science and Technology (Shenzhen, China) (Figure 1A). The laboratory features a specialized wind wall system capable of producing stable, controllable airflow conditions. The system can simulate wind shear and gust spectra corresponding to wind speeds up to 15 m/s in controlled environments. During the wind wall experiments, twelve wind speed levels were used by increasing the system power in 5% increments from 1 m/s to 10 m/s (corresponding to specific wind speeds of 1.4 m/s, 2.2 m/s, 3.0 m/s, 3.8 m/s, 4.5 m/s, 5.3 m/s, 6.1 m/s, 6.9 m/s, 7.7 m/s, 8.5 m/s, 9.2 m/s, and 10.0 m/s). Prior to testing, the wind wall output was calibrated using a high-accuracy reference anemometer to ensure measurement reliability.

Three different UAV payload configurations were tested to simulate real-world operational conditions, including a default setup with only a wind sensor (M_o), a configuration with an additional payload of approximately 1.5 kg (160 × 100 × 90 mm³, L × W × H) mounted at the front-top of the UAV (M_{o+f}), and a configuration with the same payload mounted at the center-top (M_{o+m}), as illustrated in Figure 1D. In order to assess the effects of wind direction relative to the UAV heading on attitude response and wind estimation, six wind directions were explored, including 0°, 45°, 90°, 180°, 225°, and 270°, as illustrated in Figure 1E. For each combination of wind speed and direction, the UAV maintained a stable hover for over 1 min. This procedure yielded a set of relationships between wind components and the UAV roll and pitch angles.

a. Wind estimation based on UAV attitude dynamics (method 1)

UAV tilts in the presence of wind during flights. The inclination angle (Ψ) of the UAV during flight (Figure 2) can be calculated using equation (1):

$$\Psi = arccos(cos\phi cos\theta) \tag{1}$$

where ϕ and θ are the roll (Figure 2A) and pitch (Figure 2B) angles of the UAV, respectively; $cos\phi cos\theta$ corresponds to the projection of the body-axis vertical component of the UAV onto the ground vertical axis (Z-axis) (Figure 2D).

Increasing wind speed causes the UAV to tilt. The inclination angle of the UAV, derived from its roll and pitch angles using equation (1), is therefore expected to increase with wind speed. The specific functional relationship between the inclination angle and the true wind speed can be then determined empirically by correlating the measured inclination angle with the independently controlled wind speed from the wind wall system.

For wind direction (η_{wind}), it can be estimated based on the UAV attitude using equation (2):

$$\eta_{wind} = \begin{cases} arctan(\frac{-sin\phi cos\theta}{cos\phi sin\theta}) + 180° + \delta, & if \ \theta > 0; cos\phi sin\theta > 0; \\ arctan(\frac{-sin\phi cos\theta}{cos\phi sin\theta}) + \delta, & if \ \theta < 0; cos\phi sin\theta < 0; \end{cases} \tag{2}$$

where $sin\phi cos\theta$ and $cos\phi sin\theta$ represent the wind components along the *Y*-axis and *X*-axis (Figure 2E), respectively. η_r, representing wind direction relative to UAV yaw orientation, can be obtained using equation (3):

$$\eta_r = \delta - \eta_{wind} \tag{3}$$

In this study, η_r was set to 0°, 45°, 90°, 180°, 225°, and 270° during the wind wall experiments, as illustrated previously.

b. Wind estimation based on onboard wind sensor (method 2)

Wind speed and direction data were also obtained directly from a compact and lightweight ultrasonic anemometer (LI-550 TriSonica Mini, LI-COR) mounted on the UAV airframe. The anemometer determines wind parameters by measuring ultrasonic pulse transit time differences along three orthogonal axes. The accuracy of the anemometer is ± 0.2 m/s for speeds between 0 and 10 m/s, and ± 2 % for speeds from 10 m/s to 30 m/s. The wind direction measurement range is 0 to 360°, with a manufacturer-specified sensor accuracy of ± 1°. Data were recorded at 1 Hz by an onboard datalogger during the experiments.

Prior to field deployment, the sensor underwent extensive laboratory calibration in the wind wall facility. Calibration procedures systematically tested wind speeds from 1 to 10 m/s under three payload configurations (baseline, front-loaded, and center-loaded), while also evaluating directional response at six headings relative to the UAV (Figures 1D and 1E). This process generated detailed correction curves that accounted for rotor interference and airframe effects. The resulting calibration framework ensured reliable wind data collection during subsequent field operations.

c. Wind estimation using a machine learning algorithm (method 3)

A random forest model was developed to enable efficient wind estimation. The simulations utilized the *RandomForestRegressor* from a Python package (*sci-kit learn*). The number of decision trees was set to 100 to ensure ensemble diversity. Maximum tree depth was not restricted to capture complex data patterns. An 80:20 training-test data split and 10-fold cross-validation were applied. The random seed was fixed at 42 to guarantee the reproducibility of the results.

Model training and validation employed a dataset collected during a summer field campaign at Xichong in Shenzhen, China (Figure 1C). This is a coastal site usually selected for atmosphere-land-ocean interactions. The dataset contained measurements from 20 days (from August 21 to September 14, 2022) with 6 hovering flights conducted each day, specifically

6

2 flights each during morning, afternoon, and evening periods. All flights were performed over the sea surface at distances around 100 m from land. Model inputs included UAV attitude parameters (pitch, roll, and yaw) along with supplementary flight data such as UAV flight speed, rotor thrusts, and air pressure. UAV flight speed was derived from onboard GPS measurements, and rotor thrusts were approximated from flight command values (Text S1, Supporting Information). The training targets were obtained from calibrated onboard ultrasonic anemometer measurements (method 2), with performance benchmarks established through comparison against attitude-based wind estimation (method 1). Performance of the random forest estimation was evaluated using the correlation coefficient (R^2) and root mean squared error (RMSE).

2.3 UAV wind estimation validation

Validation of UAV wind estimation was conducted at the Shiyan Meteorological Gradient Observation Tower in Shenzhen, China (Figure 1B). The tower features 13 external platforms for conventional meteorological measurements. Meteorological measurement platforms are distributed across levels at 10 m, 20 m, 40 m, 50 m, 80 m, 100 m, 150 m, 160 m, 200 m, 250 m, 300 m, 320 m, and 350 m above local ground, providing multi-level wind speed and direction data. Due to flight restrictions in the area where the maximum permissible height was 120 m, flight experiments were conducted within 100 m. Both hovering and vertical flight profiles were performed. For the hovering experiment, UAV with the default payload configuration (M_o) maintained a stationary position for approximately 10 min at an altitude of 100 m above ground level. The vertical flight experiments assessed two payload configurations (M_o and M_{o+f}) at ascent/descent speeds of 0.5 m/s and 2.0 m/s. For each configuration and speed, two complete round-trip cycles were performed, ascending from ground level to 100 m and descending back to 0 m. All UAV flights were conducted at a minimum horizontal distance of 20 m from the tower to avoid the disturbance of UAV-induced air flows to the tower measurements.

3. Results and Discussion

3.1 UAV-based wind estimation

a. Estimation based on UAV attitude dynamics (method 1)

Accurate and fast UAV attitude-based wind estimation requires UAV attitude to respond rapidly to wind change. As shown in Figure S1, which plots inclination angle and controlled wind speed against time for a test flight, wind speed was increased in a stepwise fashion at 15-s intervals. The data, sampled at 1-s intervals, show that the UAV attitude (quantified by the inclination angle) adjusts to each new wind speed level within the first second of the change. This rapid response is evident across all step increments and becomes particularly pronounced at higher wind speeds, indicating a transient response time on the order of 1 s or less for this platform when reacting to a sudden change in wind forcing.

The relationship between UAV inclination angle and wind speed was then modelled using datasets collected under different loading conditions (M) and relative wind directions (η_r), as presented in Figure 3. Several fitting algorithms were

evaluated, including power, logarithmic power, polynomial, and exponential functions. Among these, the power function demonstrated the best fit to the experimental data, which is expressed as:

$$V_{wind,M,\eta_r} = a_{M,\eta_r} \Psi^{b_{M,\eta_r}} \tag{4}$$

where a_{M,η_r} and b_{M,η_r} are fitting coefficients obtained from the wind wall experiments. Overall, the fittings effectively captured the relationship between UAV inclination angle and wind speed ($R^2 > 0.85$, Table S1).

As shown in Figure 3, the relationship between UAV inclination angle and wind speed varies significantly with relative wind direction. At identical wind speeds, inclination angles remained smaller for headwind to crosswind conditions (0°-90°) than for tailwind to rear crosswind scenarios (180°-270°). This behavior can be attributed to the advanced flight control system of the UAV used in this study. Under headwind conditions, the flight controller proactively compensates for wind disturbances by precisely adjusting front rotor power, inducing a slight forward tilt. This active posture control leverages aerodynamic drag components to enhance stability, thereby minimizing attitude fluctuations (Ding and Wang, 2018; Otsuka et al., 2018; Lei and Lin, 2019; Jung, 2024). Conversely, during tailwind conditions, turbulent flow enveloping the airframe introduces control latency, forcing the system to apply larger attitude corrections to maintain position, ultimately amplifying the observed inclination (Ding and Wang, 2018; Otsuka et al., 2018; Lei and Lin, 2019; Jung, 2024). Adding extra payload generally reduces how sensitive the UAV inclination is to wind, leading to smaller observed inclination angles (Figures 3B and 3C versus Figure 3A). This effect varies slightly depending on payload placement.

The above findings differ from observations by Neumann and Bartholmai (2015), who reported that payload and wind direction had minimal effects on UAV attitude. This discrepancy likely stems from differences in UAV platforms, including variations in design and flight control architectures. The implication is that UAV attitude-based wind estimation requires specific algorithms tailored to the characteristics of each UAV platform.

b. Estimation based on onboard wind sensor (method 2)

The wind sensor was also calibrated during wind wall experiments. Across varying payload configurations and wind directions, linear relationships were consistently observed between sensor-measured wind speeds and the reference wind speeds generated by the wind wall (Figure 4). The coefficients of these linear fits are provided in Table S2.

As shown in Figure 4, sensor measurements exhibited deviations of 30%, 15%, and 30% for the default, front payload, and central payload configurations, respectively. The front payload configuration notably improved measurement accuracy by reducing flight vibrations and enhancing stability (Figure 4B versus Figures 4A and 4C), consistent with the UAV flight control system behavior described in Section 3.1a. In addition, the asymmetric sensor placement on the right front of the UAV (viewed when facing the UAV, Figure 1E) led to maximum accuracy degradation at 225° (rear direction relative to the UAV centerline) and secondary effects at 45° (head direction relative to the centerline).

Over the course of the experiments, the sensor registered non-zero wind speed readings even when the actual external wind speed was 0 m/s. The intercepts of the calibration curves for different flight configurations represent the zero bias (Figure 4). This phenomenon can be attributed to the rotor-induced airflow interference. During testing under various payload configurations and wind directions, UAV rotors generated apparent wind speeds ranging from 0.1 to 1.5 m/s (Figure 4). Similarly, the rotor interference effects on sensor measurements were most pronounced when wind approached from the right rear (225°) and head (45°) directions relative to the UAV centerline, likely due to uneven payload distribution.

The implication of these findings is that the sensor cannot be used for field measurements without calibration, and calibration may vary significantly with UAV model used, sensor placement, payload distribution and mass, and relative wind direction during operation.

3.2 Validation of UAV-based wind estimation against tower measurements

Results of hovering flight experiments conducted at the meteorological observation tower are presented in Figure 5. Wind speeds obtained from method 1 (UAV-attitude based) and method 2 (sensor-based) were generally consistent with each other (Figure 5A). Both methods also closely matched the reference wind speed and direction recorded by the tower-mounted anemometers (Figures 5B and 5C). The RMSE between the two measurement methods and the anemometer readings was less than 0.7 m/s (for wind speed) and 20° (for wind direction), confirming the accuracy and reliability of UAV-based wind estimation under real-world atmospheric conditions.

However, the situation changes during vertical flight operations. In this study, vertical flights were conducted at speeds of 0.5 m/s and 2 m/s. As shown in Figure 6, wind speeds calculated using method 1 still exhibit strong agreement with meteorological tower measurements, regardless of whether the UAV ascends or descends at 0.5 m/s (Figure 6A-I) or 2.0 m/s (Figure 6B-I). For the sensor-based method (method 2), the measurements matched the tower data at the lower vertical speed (0.5 m/s, Figure 6A-II). However, when the vertical speed increased to 2.0 m/s, significant deviations became apparent (Figure 6B-II). These discrepancies are likely caused by increased rotor-induced turbulence during high-speed vertical flight, which degrades sensor measurement accuracy. Notably, the addition of payload had no effect on the wind estimation accuracy when using method 1 (Figures 6B-I versus 6D-I), while it amplified the impact of rotor-induced airflow disturbances on sensor measurements (Figures 6B-II versus 6D-II). Similar findings were observed for wind direction estimations (Figure S2).

These comprehensive analyses demonstrate that the attitude-derived method (method 1) can robustly estimate wind variables. For the sensor-based method (method 2), results indicate that with proper calibration, the sensors can achieve accuracy comparable to commercial meteorological instruments during UAV hovering and low-speed vertical profiling. However, the sensor-based method shows limitations for high-speed vertical profiling due to its significant susceptibility to rotor-induced airflow disturbances. These systematic errors were consistently observed across all test configurations. Nevertheless, the successful validation of the attitude-based method substantially enhances the potential for UAV applications

in atmospheric research, offering distinct advantages for measurements in locations inaccessible to conventional tower-based systems and in scenarios requiring rapid deployment of mobile platforms.

3.3 Field wind measurements

Field flight experiments were further conducted at a coastal site in Shenzhen, China, to evaluate the wind estimation performance of methods 1 and 2. Figure 7 presents the results for UAV hovering data. Strong agreement was observed between the two methods, with median differences of approximately 0.1 m/s for wind speed and less than 10° for wind direction (Figures 7A and S3), confirming the reliability of the UAV attitude-based approach.

To further enhance the wind estimation, we implemented a machine learning framework (method 3) using UAV attitude parameters and supplementary flight data as inputs, with corrected wind sensor measurements as the training target. The model achieved excellent predictive performance, with R^2 values exceeding 0.90 for both training and test datasets (Figures 7B and S4). For hovering flights, roll, pitch, yaw, and pressure were identified as the most important features. When applied to an independent dataset from the meteorological tower flight experiments (Section 3.3), the estimates maintained good agreement with tower measurements (Figure S5).

Similar performance was achieved for UAV vertical flights (Figure S6). In vertical profiling, in addition to input variables discussed above, vertical flight speed and rotor thrusts became more significant for the machine learning estimates. It should be noted that the rotor thrust information was only roughly estimated from flight command values issued by the UAV controller in this study, which may introduce significant uncertainty. Future research applying a machine learning approach for wind estimation should therefore seek to incorporate actual rotor thrust or rotor speed data to improve accuracy. Furthermore, as this study focuses only on hovering and vertical flights, horizontal velocity components were not included in the model. For future applications of this approach to horizontal flight, horizontal velocity in the x- and y-directions should also be integrated into the model to account for the UAV motion relative to the air. Nevertheless, the above consistent performance across different validation approaches and flight modes confirms the robustness of the UAV attitude-based methodology and its potential for practical wind measurement applications.

Wind profile estimation offers critical insights into atmospheric pollutant transport and dispersion dynamics. Using the field campaign data as an example, we constructed diurnal vertical wind profiles by analyzing UAV attitude variations during flights. In the field campaign, we also collected vertical pollutant concentration profiles using a pre-calibrated sensor package (Sniffer V2, Soarability Pte. Ltd.), with cross-validation against reference instruments at a ground station located 50 m from the flight site. The UAV vertical flight speed was maintained at approximately 0.5 m/s and only ascending flight data were used to minimize the influence of rotor downwash on sensor measurements.

Representative vertical profiles of both wind and pollutant measurements are displayed in Figure 8, which reveals the crucial influence of wind profiles on pollutant distribution patterns. For instance, persistently low wind speeds were observed

throughout the day of August 23, indicating stable atmospheric conditions which were conducive to pollution accumulation. Pollutant concentrations in this day exhibited typical diurnal variations, gradually increasing from morning, peaking in the afternoon due to photochemical activity, and decreasing at night with reduced emissions and photochemical processes. In contrast, September 7 featured strong winds that enhanced pollutant dispersion, resulting in consistently low pollution levels.

The September 14 case demonstrated a complex vertical wind structure, with speeds decreasing from morning to nighttime minima while increasing with height. Pollutant concentrations varied significantly with wind direction changes. Notably, at 19:00, a 180° wind shift transported polluted air masses from the south, sharply increasing observed concentrations. Surface cooling and calm winds at this night created stable stratification, trapping pollutants near the surface and producing distinct vertical gradients. The nocturnal boundary layer height (150-200 m), identifiable from wind and pollutant profiles (Guimarães et al., 2019, 2020; Ye et al., 2021), showed reduced pollutant concentrations at the residual layer due to enhanced wind speed and dispersion. A subsequent wind shift to 360° brought back cleaner northern air, reducing both surface concentrations and vertical gradients. These observations underscore the importance of vertical wind profiling enabled by UAV-attitude-based estimation, for understanding atmospheric transport mechanisms and pollution dynamics.

4. Atmospheric Implications

This study develops a UAV wind estimation method based on attitude changes. Validation through wind wall and field experiments demonstrated the reliable performance of the attitude-based approach. Key findings indicate that payload variations significantly affect attitude responses, with distinct patterns observed across different wind directions, underscoring the importance of comprehensive training data to improve model accuracy. We further developed a supervised learning framework to extract wind parameters directly from UAV attitude and supplementary flight data. The machine learning model achieved accurate predictions of both wind speed and direction while maintaining practicality for field deployment. Compared to the attitude-based approach, the results revealed significant rotor-induced interference when using onboard sensors for wind measurement, particularly during vertical maneuvers. This highlights the need for pre-deployment calibration and bias corrections for sensor measurements. Collectively, these results demonstrate the strong potential for precise, sensor-free wind field estimation using UAV attitude data.

The UAV attitude-based wind estimation method, while promising, presents several limitations that require future consideration. First, this approach requires establishing accurate relationships between UAV inclination angles and wind speed, which vary across different UAV models. For instance, the platform used in this study exhibited significant effects from payload and relative wind direction, a phenomenon not reported by Neumann and Bartholmai (2015) for a different UAV. Consequently, model-specific calibration is essential prior to field deployment. In this work, we selected the DJI M300 RTK (total weight 6.3 kg, maximum payload 2.3 kg) as it represents a class of small-sized rotorcraft capable of carrying scientific payloads such as wind sensors (Li et al., 2025). Different UAV categories present distinct trade-offs. Mini-UAVs (weight < 3

11

kg), while potentially suitable for low-wind conditions, often lack the payload capacity for full instrumentation and can be overly sensitive to turbulence, increasing estimation uncertainty. Conversely, larger platforms (e.g., agricultural UAVs) are heavier and exhibit a dampened attitude response, making them more stable in high winds; however, in low- to moderate-wind conditions, their significant rotor-induced airflow may dominate the measured signal, degrading fidelity. Thus, platform selection should be guided by the target wind regime and payload requirements, with the understanding that each configuration demands its own calibration.

Additionally, this study identified greater uncertainty in the attitude-based wind speed estimates below 2 m/s under headwind conditions (e.g., 45° to 90°, Figure 3, likely owing to the advanced UAV flight control system described in Section 3.1). To address this challenge, future research could explore hybrid approaches integrating attitude-derived estimates with measurements from pre-calibrated onboard sensors, thereby enhancing accuracy in low-wind-speed regimes. It should be noted that strong vertical winds, for example, from intense thermal convection and terrain-induced uplift, may also affect UAV attitude and, consequently, wind estimation. This effect can be more pronounced under low horizontal wind conditions, where vertical disturbances can induce significant platform vibration. Under typical open-field atmospheric conditions, however, where vertical wind speeds are on the order of 0.01 to 0.1 m/s (Lynch and Cassano, 2006; Michaelides et al., 2019), such influences are expected to be minor. The close agreement between the tower-based (or calibrated sensor) measurements and the UAV attitude-based estimates (Figures 6 and 7) further supports the conclusion that interference is limited. Furthermore, the UAV's own rotor-induced vertical velocities, which can exceed several m/s for platforms such as DJI M300 RTK (Li et al., 2025) and are often substantially larger than typical ambient vertical wind speeds, dominate the vertical momentum balance and mask weaker atmospheric updrafts or downdrafts. Nevertheless, future research focused on UAV wind estimation in environments with significant vertical flows, such as urban street canyons, mountainous terrain with intense slope winds, or severe weather fronts, should explicitly account for the influence of vertical winds on UAV dynamics and sensor measurements to ensure accurate retrievals.

Finally, creating a comprehensive database linking UAV attitude data to wind measurements across diverse flight conditions (e.g., hovering, horizontal, and vertical flight at varying speeds) and environmental scenarios would be highly valuable. In complex terrains such as urban canyons or under unstable atmospheric conditions, the wind itself can be complex, inducing turbulence and wind shear that significantly affect UAV attitude and may introduce uncertainty in UAV-based wind estimates. A dataset encompassing such varied conditions would enable the training of more advanced AI models, accelerating the development of reliable, attitude-based wind field prediction methods. Although previous studies have applied machine learning to train wind observation data (e.g., Zhu et al., 2025), they have typically been constrained by single-flight tests or limited datasets, which fail to capture the full variability of UAV responses across different operating environments. In practice, UAV attitude and rotor dynamics are strongly modulated by wind direction, flight mode, and payload configuration, leading to highly nonlinear and platform-specific responses, as demonstrated in this study. Expanding datasets and integrating physical

340 knowledge of UAV aerodynamics into data-driven models will therefore be essential for building more robust and transferable AI-based wind sensing frameworks.

With the global development of the low-altitude economy (Huang et al., 2024; Saadé et al., 2025; Tan et al., 2025; Zhou, 2025), UAV attitude-based wind estimation has become an essential enabling technology. The sensor-free approach described here uses inherent flight dynamics to generate reliable wind field data, offering advantages in low-altitude operations where
345 conventional methods are limited. Its operational simplicity and cost-effectiveness make it valuable for widespread use in sectors such as urban air mobility, where it can support flight safety by integrating easily into existing UAV systems.

In environmental applications, UAVs provide precise, flexible, and efficient wind measurements with high spatiotemporal resolution. This enables vertical wind profiling, improving the analysis of atmospheric pollutant transport. Such data can help identify pollution sources and inform mitigation strategies, especially in complex urban settings where building
350 layouts and street-level airflow affect air quality. The three-dimensional wind data obtained from UAV measurements can inform urban planning decisions by characterizing how architectural geometries modulate near-surface ventilation efficiency. Furthermore, the measurement capabilities provide critical data for validating high-resolution weather and climate models, especially for simulating complex urban canopy effects on microscale wind circulation patterns that govern heat dissipation.

Beyond urban research, UAV-based wind estimation opens new opportunities for field studies in natural ecosystems and
355 remote regions. For example, reliable vertical wind profiles can substantially improve the quantification of forest canopy-atmosphere exchange processes, including the dispersion of biogenic volatile organic compounds and greenhouse gases (Jiang et al., 2024; Ye et al., 2021). Similarly, accurate wind field characterization over coastal and marine environments enhances the interpretation of air-sea exchange fluxes, sea-breeze circulation, and the long-range transport of marine aerosols (Zhao et al., 2021). For atmospheric chemistry studies, UAV-derived wind fields provide essential inputs for constraining dispersion
360 models and for interpreting aircraft or ground-based observations, particularly in regions where conventional meteorological measurements are sparse or absent (Ye et al., 2022).

Through these varied applications, UAV-based wind measurement technology is emerging as an innovative tool that connects the low-altitude economy with environmental science. By delivering spatiotemporally resolved wind data in complex terrains and under diverse atmospheric conditions, the approach not only advances intelligent environmental risk management
365 but also supports sustainable development initiatives and climate adaptation strategies on regional to global scales.

Supporting Information. The supporting information includes the following items:

Text S1   Estimation of UAV rotor thrusts

Table S1   Fitting coefficients for the UAV inclination-wind speed relationships.

Table S2   Fitting coefficients k and b for wind sensor calibrations under various flight conditions.

Figure S1   UAV attitude response to a step change in wind speed.

Figure S2   Comparison between UAV-based wind direction estimates and reference measurements from the meteorological observation tower during vertical flight operations.

Figure S3   UAV-based wind direction estimation and deviation analysis comparing different methods from the field observation campaign.

Figure S4   Performance of wind estimation using machine learning algorithms for hovering flights.

Figure S5   Comparison between UAV-attitude-based wind speed estimates using machine learning algorithms and reference measurements from the meteorological observation tower during hovering flight operations.

Figure S6   Performance of wind estimation using machine learning algorithms for vertical flights. And comparison between UAV-attitude-based wind speed estimates using machine learning algorithms and reference measurements from the meteorological observation tower during vertical flight operations.

Corresponding Author. Jianhuai Ye (yejh@sustech.edu.cn), ORCID: 0000-0002-9063-3260

Author Contribution. J.Y. designed the research; D.C., W.S., S.J., Y.L. and J.Y. conducted wind wall and meteorological tower flight experiments; S.J. and J.Y. performed the UAV field campaign; D.C. and J.Y. analyzed the data and wrote the original manuscript; all authors contributed to the data interpretation and manuscript writing.

Competing Interest. The authors declare no competing financial interest.

References

Achermann, F., Stastny, T., Danciu, B., Kolobov, A., Chung, J. J., Siegwart, R., and Lawrance, N.: WindSeer: real-time volumetric wind prediction over complex terrain aboard a small uncrewed aerial vehicle, Nat. Commun., 15, 3507, https://doi.org/10.1038/s41467-024-47778-4, 2024.

Ahmed, Z., Halefom, M. H., and Woolsey, C.: Tutorial review of indirect wind estimation methods using small uncrewed air vehicles, J. Aerosp. Inf. Syst., 21, 667-683, https://doi.org/10.2514/1.I011345, 2024.

Alfonso-Corcuera, D., Ogueta-Gutiérrez, M., Fernández-Soler, A., González-Bárcena, D., and Pindado, S.: Measuring relative wind speeds in stratospheric balloons with cup anemometers: the TASEC-lab mission, Sensors, 22, 5575, https://doi.org/10.3390/s22155575, 2022.

Alizadeh, O., Abniki, M., Babaei, M., and Irannejad, P.: Climatology and the dynamic mechanism of the levar wind and dust events in eastern Iran, Int. J. Climatol., 42, 9288-9303, https://doi.org/10.1002/joc.7818, 2022.

Asher, E., Hills, A. J., Hornbrook, R. S., Shertz, S., Gabbard, S., Stephens, B. B., Helmig, D., and Apel, E. C.: Unpiloted aircraft system instrument for the rapid collection of whole air samples and measurements for environmental monitoring and air quality studies, Environ. Sci. Technol., 55, 5657-5667, https://doi.org/10.1021/acs.est.0c07213, 2021.

Batista, C. E., Ye, J., Ribeiro, I. O., Guimarães, P. C., Medeiros, A. S. S., Barbosa, R. G., Oliveira, R. L., Duvoisin, S., Jardine, K. J., Gu, D., Guenther, A. B., McKinney, K. A., Martins, L. D., Souza, R. A. F., and Martin, S. T.: Intermediate-scale horizontal isoprene concentrations in the near-canopy forest atmosphere and implications for emission heterogeneity, Proc. Natl. Acad. Sci., 116, 19318-19323, https://doi.org/10.1073/pnas.1904154116, 2019.

Brosy, C., Krampf, K., Zeeman, M., Wolf, B., Junkermann, W., Schäfer, K., Emeis, S., and Kunstmann, H.: Simultaneous multicopter-based air sampling and sensing of meteorological variables, Atmos. Meas. Tech., 10, 2773-2784, https://doi.org/10.5194/amt-10-2773-2017, 2017.

Curbelo, J. and Rypina, I. I.: A three dimensional lagrangian analysis of the smoke plume from the 2019/2020 Australian wildfire event, J. Geophys. Res. Atmos., 128, e2023JD039773, https://doi.org/10.1029/2023JD039773, 2023.

Diasinos, S., Beves, C., and Barber, T.: Alignment technique for three-dimensional laser doppler anemometry, Meas. Sci. Technol., 24, 17001, https://doi.org/10.1088/0957-0233/24/1/017001, 2013.

Ding, L. and Wang, Z.: A robust control for an aerial robot quadrotor under wind gusts, J. Robot., 2018, 1-8, https://doi.org/10.1155/2018/5607362, 2018.

Feng, Y., Fu, D., Zhao, Z., Zong, W., Yu, T., Sheng, Z., and Zhu, Y.: An overview of spaceborne atmospheric wind field measurement with passive optical remote sensing, Acta Opt. Sin., 43, 0601011, https://doi.org/10.3788/AOS221462, 2023.

Gaeta Lopes, G. M., da Silva Junior, D. P., de Franca, J. A., de Morais Franca, M. B., Ribeiro, L. de S., Moreira, M., and Elias, P.: Development of 3-D ultrasonic anemometer with nonorthogonal geometry for the determination of high-intensity winds, IEEE Trans. Instrum. Meas., 66, 2836-2844, https://doi.org/10.1109/TIM.2017.2714438, 2017.

González-Rocha, J., Woolsey, C. A., Sultan, C., and De Wekker, S. F. J.: Sensing wind from quadrotor motion, J. Guid. Control Dyn., 42, 836-852, https://doi.org/10.2514/1.G003542, 2019.

González-Rocha, J., Bilyeu, L., Ross, S. D., Foroutan, H., Jacquemin, S. J., Ault, A. P., and Schmale, D. G.: Sensing atmospheric flows in aquatic environments using a multirotor small uncrewed aircraft system (sUAS), Environ. Sci. Atmos., 3, 305-315, https://doi.org/10.1039/D2EA00042C, 2023.

Guimarães, P., Ye, J., Batista, C., Barbosa, R., Ribeiro, I., Medeiros, A., Souza, R., and Martin, S. T.: Vertical profiles of ozone concentration collected by an unmanned aerial vehicle and the mixing of the nighttime boundary layer over an Amazonian urban area, Atmosphere, 10, 599, https://doi.org/10.3390/atmos10100599, 2019.

Guimarães, P., Ye, J., Batista, C., Barbosa, R., Ribeiro, I., Medeiros, A., Zhao, T., Hwang, W.-C., Hung, H.-M., Souza, R., and T. Martin, S.: Vertical profiles of atmospheric species concentrations and nighttime boundary layer structure in the dry season over an urban environment in central Amazon collected by an unmanned aerial vehicle, Atmosphere, 11, 1371, https://doi.org/10.3390/atmos11121371, 2020.

Guo, J., Miao, Y., Zhang, Y., Liu, H., Li, Z., Zhang, W., He, J., Lou, M., Yan, Y., Bian, L., and Zhai, P.: The climatology of planetary boundary layer height in China derived from radiosonde and reanalysis data, Atmos. Chem. Phys., 16, 13309-13319, https://doi.org/10.5194/acp-16-13309-2016, 2016.

Han, D., Kim, S., and Park, S.: Two-dimensional ultrasonic anemometer using the directivity angle of an ultrasonic sensor, Microelectron. J., 39, 1195-1199, https://doi.org/10.1016/j.mejo.2008.01.090, 2008.

Hauser, D., Abdalla, S., Ardhuin, F., Bidlot, J.-R., Bourassa, M., Cotton, D., Gommenginger, C., Evers-King, H., Johnsen, H., Knaff, J., Lavender, S., Mouche, A., Reul, N., Sampson, C., Steele, E. C. C., and Stoffelen, A.: Satellite remote sensing of surface winds, waves, and currents: where are we now?, Surv. Geophys., 44, 1357-1446, https://doi.org/10.1007/s10712-023-09771-2, 2023.

Horton, D. E., Skinner, C. B., Singh, D., and Diffenbaugh, N. S.: Occurrence and persistence of future atmospheric stagnation events, Nat. Clim. Change, 4, 698-703, https://doi.org/10.1038/nclimate2272, 2014.

Huang, H., Su, J., and Wang, F.-Y.: The potential of low-altitude airspace: the future of urban air transportation, IEEE Trans. Intell. Veh., 9, 5250-5254, https://doi.org/10.1109/TIV.2024.3483889, 2024.

Jiang, S., Wang, Y., Huang, X., Liu, B., Nie, D., Ge, Y., Ma, L., Wang, Q., Wang, J., Ma, Y., Jiang, S., Shu, Z., Zhang, Y., Sun, J., Wu, C., Ge, X., Zhu, L., Shen, H., Wang, C., Zheng, Y., Fu, T.-M., Yang, X., Li, Y. J., Chen, Q., and Ye, J.: Characteristics of nocturnal boundary layer over a subtropical forest: implications for the dispersion and fate of atmospheric species, Environ. Sci. Technol., 58, 23075-23087, https://doi.org/10.1021/acs.est.4c05051, 2024.

Jung, S.: Precision landing of unmanned aerial vehicle under wind disturbance using derivative sliding mode nonlinear disturbance observer-based control method, Aerospace, 11, 265, https://doi.org/10.3390/aerospace11040265, 2024.

Knöller, W., Bagheri, G., Von Olshausen, P., and Wilczek, M.: Analysis of the measurement uncertainty for a 3D wind lidar, Atmos. Meas. Tech., 17, 6913-6931, https://doi.org/10.5194/amt-17-6913-2024, 2024.

Lee, B.: Review of the present status of optical fiber sensors, Opt. Fiber Technol., 9, 57-79, https://doi.org/10.1016/S1068-5200(02)00527-8, 2003.

Lei, Y. and Lin, R.: Effect of wind disturbance on the aerodynamic performance of coaxial rotors during hovering, Meas. Control, 52, 665-674, https://doi.org/10.1177/0020294019834961, 2019.

Li, Y., Zhang, C., Su, W., Jiang, S., Nie, D., Wang, Y., Wang, Y., He, H., Chen, Q., Martin, S. T., and Ye, J.: Copter-type UAV-based sensing in atmospheric chemistry: recent advances, applications, and future perspectives, Environ. Sci. Technol., 59, 13532-13550, https://doi.org/10.1021/acs.est.5c00074, 2025.

Liu, J., Zhao, Z., Fang, Z., Li, Y., and Du, L.: Correction of error of airborne anemometers caused by self-excited air turbulence, Sensors, 23, 4288, https://doi.org/10.3390/s23094288, 2023.

Lynch, A. H. and Cassano, J. J.: Applied Atmospheric Dynamics, John Wiley & Sons, Hoboken, NJ, USA, 2006.

Michaelides, S., Lane, J., and Kasparis, T.: Effect of vertical air motion on disdrometer derived Z-R coefficients, Atmosphere, 10, 77-98, https://doi.org/10.3390/atmos10020077, 2019.

Neumann, P. P. and Bartholmai, M.: Real-time wind estimation on a micro unmanned aerial vehicle using its inertial measurement unit, Sens. Actuators Phys., 235, 300-310, https://doi.org/10.1016/j.sna.2015.09.036, 2015.

Otsuka, H., Sasaki, D., and Nagatani, K.: Reduction of the head-up pitching moment of small quad-rotor unmanned aerial vehicles in uniform flow, Int. J. Micro Air Veh., 10, 85-105, https://doi.org/10.1177/1756829317745318, 2018.

Palomaki, R. T., Rose, N. T., Van Den Bossche, M., Sherman, T. J., and De Wekker, S. F. J.: Wind estimation in the lower atmosphere using multirotor aircraft, J. Atmos. Ocean. Technol., 34, 1183-1191, https://doi.org/10.1175/JTECH-D-16-0177.1, 2017.

Pindado, S., Cubas, J., and Sorribes-Palmer, F.: The cup anemometer, a fundamental meteorological instrument for the wind energy industry. Research at the IDR/UPM institute, Sensors, 14, 21418-21452, https://doi.org/10.3390/s141121418, 2014.

Richiardone, R., Manfrin, M., Ferrarese, S., Francone, C., Fernicola, V., Gavioso, R. M., and Mortarini, L.: Influence of the sonic anemometer temperature calibration on turbulent heat-flux measurements, Bound.-Layer Meteorol., 142, 425-442, https://doi.org/10.1007/s10546-011-9688-z, 2012.

Saadé, R. G., Hao, L., and Kuusiholma, T.: Global governance & aerospace - the need for a management-integrated air and space education paradigm, J. Space Saf. Eng., 12, 17-27, https://doi.org/10.1016/j.jsse.2025.04.003, 2025.

Salmabadi, H., Khalidy, R., and Saeedi, M.: Transport routes and potential source regions of the Middle Eastern dust over Ahvaz during 2005-2017, Atmos. Res., 241, 104947, https://doi.org/10.1016/j.atmosres.2020.104947, 2020.

Shan, Z., Xie, X., and Liu, X.: Wind speed and direction measurement based on three mutually transmitting ultrasonic sensors, IEEE Geosci. Remote Sens. Lett., 20, 8000205, https://doi.org/10.1109/LGRS.2023.3236005, 2023.

Sikkel, L. N. C., de Croon, G. C. H. E., De Wagter, C., and Chu, Q. P.: A novel online model-based wind estimation approach for quadrotor micro air vehicles using low cost MEMS IMUs, in: 2016 IEEE/RSJ International Conference on Intelligent Robots and Systems (IROS), pp. 2141-2146, https://doi.org/10.1109/IROS.2016.7759336, 2016.

Tan, H., Guo, Z., Yan, J., Zhang, D., Chen, Y., and Zhang, H.: Advancing low-carbon smart cities: leveraging UAVs-enabled low-altitude economy principles and innovations, Renew. Sustain. Energy Rev., 222, 115942, https://doi.org/10.1016/j.rser.2025.115942, 2025.

Tominaga, Y. and Shirzadi, M.: Wind tunnel measurement of three-dimensional turbulent flow structures around a building group: impact of high-rise buildings on pedestrian wind environment, Build. Environ., 206, 108389, https://doi.org/10.1016/j.buildenv.2021.108389, 2021.

Wang, H.-J. and Chen, H.-P.: Understanding the recent trend of haze pollution in eastern China: roles of climate change, Atmos. Chem. Phys., 16, 4205-4211, https://doi.org/10.5194/acp-16-4205-2016, 2016.

Yang, J., Wu, L., Li, R., Liu, X., and Tao, C.: Effects of surrounding urban morphology and wind direction on hazardous gas dispersion from chemical plants: morphological analysis and fluid dynamics insights into industry-urban interactions, Phys. Fluids, 37, 27103, https://doi.org/10.1063/5.0251016, 2025a.

Yang, Y., Russell, L. M., Lou, S., Liu, Y., Singh, B., and Ghan, S. J.: Rain-aerosol relationships influenced by wind speed, Geophys. Res. Lett., 43, 2267-2274, https://doi.org/10.1002/2016GL067770, 2016.

Yang, Y., Russell, L. M., Lou, S., Liao, H., Guo, J., Liu, Y., Singh, B., and Ghan, S. J.: Dust-wind interactions can intensify aerosol pollution over eastern China, Nat. Commun., 8, 15333, https://doi.org/10.1038/ncomms15333, 2017.

Yang, Y., Zhang, Y., Han, T., Xie, C., Liu, Y., Huang, Y., Zhou, J., Sun, H., Zhao, D., Zhang, K., and Li, S.-M.: A correction algorithm for rotor-induced airflow and flight attitude changes during three-dimensional wind speed measurements made from a rotary unoccupied aerial vehicle, Atmos. Meas. Tech., 18, 3035-3050, https://doi.org/10.5194/amt-18-3035-2025, 2025b.

Ye, J., Batista, C. E., Guimarães, P. C., Ribeiro, I. O., Vidoudez, C., Barbosa, R. G., Oliveira, R. L., Ma, Y., Jardine, K. J., Surratt, J. D., Guenther, A. B., Souza, R. A. F., and Martin, S. T.: Near-canopy horizontal concentration heterogeneity of semivolatile oxygenated organic compounds and implications for 2-methyltetrols primary emissions, Environ. Sci. Atmos., 1, 8-20, https://doi.org/10.1039/D0EA00006J, 2021.

Ye, J., Batista, C. E., Zhao, T., Campos, J., Ma, Y., Guimarães, P., Ribeiro, I. O., Medeiros, A. S. S., Stewart, M. P., Vilà-Guerau De Arellano, J., Guenther, A. B., Souza, R. A. F. D., and Martin, S. T.: River winds and transport of forest

volatiles in the Amazonian riparian ecoregion, Environ. Sci. Technol., 56, 12667-12677, https://doi.org/10.1021/acs.est.1c08460, 2022.

Zhao, T., Ye, J., Ribeiro, I. O., Ma, Y., Hung, H.-M., Batista, C. E., Stewart, M. P., Guimarães, P. C., Vilà-Guerau De Arellano, J., De Souza, R. A. F., Guenther, A. B., and Martin, S. T.: River winds and pollutant recirculation near the Manaus city in the central Amazon, Commun. Earth Environ., 2, 205, https://doi.org/10.1038/s43247-021-00277-6, 2021.

Zhou, Y.: Unmanned aerial vehicles based low-altitude economy with lifecycle techno-economic-environmental analysis for sustainable and smart cities, J. Clean. Prod., 499, 145050, https://doi.org/10.1016/j.jclepro.2025.145050, 2025.

Zhu, S., Zhao, T., Zhang, H., Chen, Y., Yang, D., Liu, Y., and Cao, J.: UAVs' flight dynamics is all you need for wind speed and direction measurement in air, Drones, 9, 466, https://doi.org/10.3390/drones9070466, 2025.
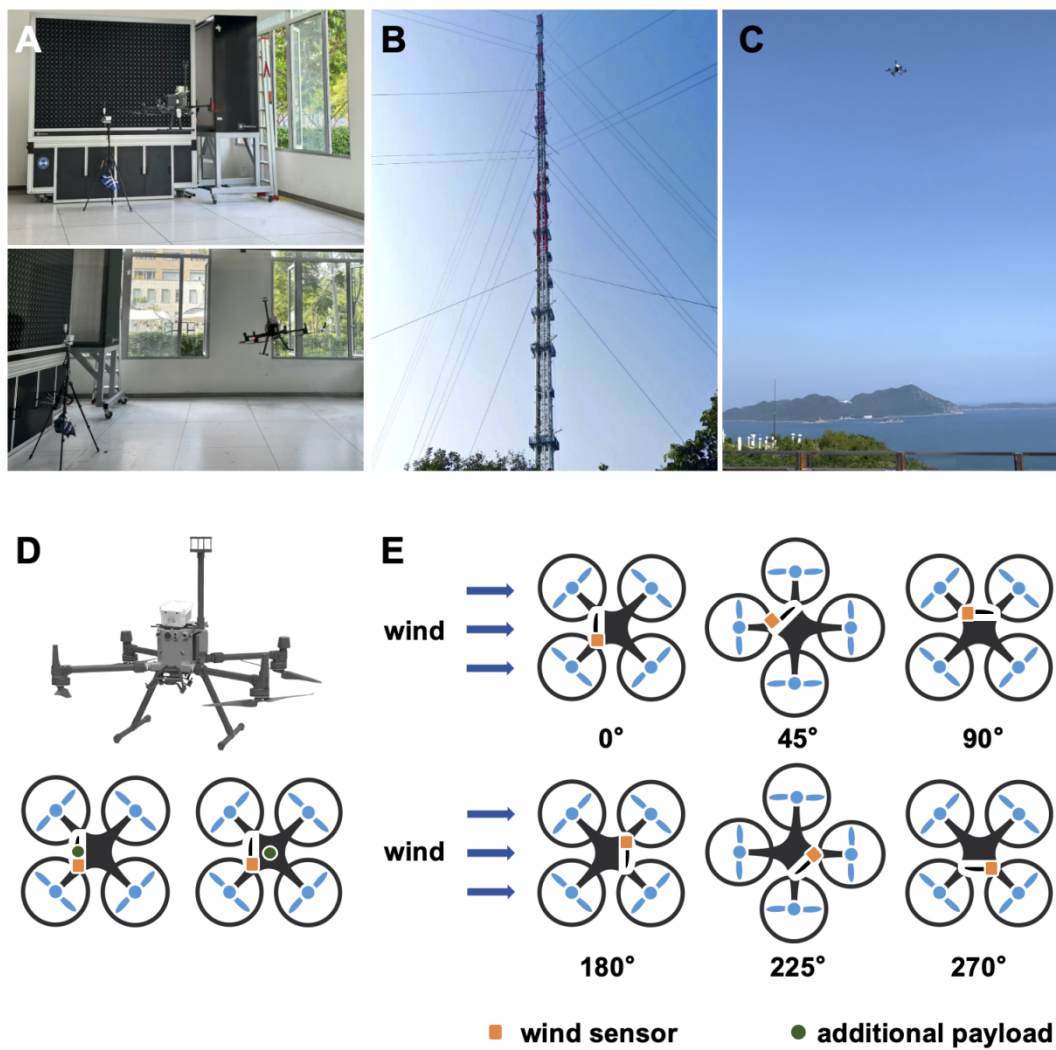
Figure 1 UAV flights conducted in a wind wall laboratory (A), at a meteorological observation tower (B), and at a coastal site (C). Picture and schematic diagrams of UAV payload configuration (D) and UAV flights under different relative wind directions (E).
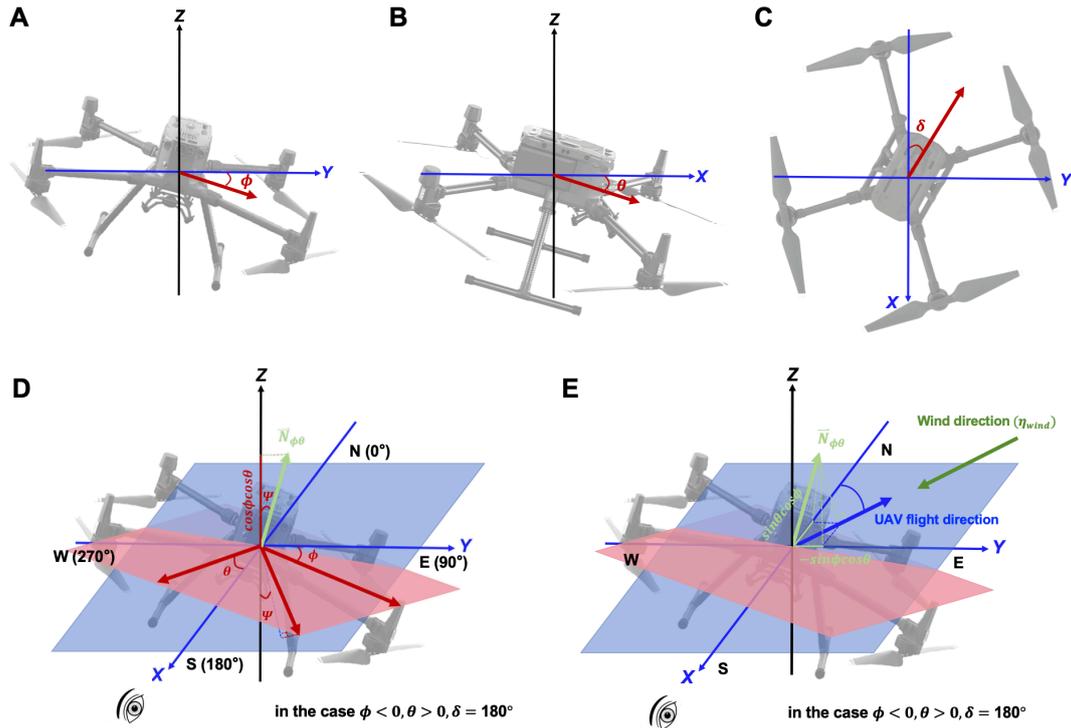
Figure 2 Schematic diagrams of UAV attitude coordinates. Panels depict (A) roll (ϕ), (B) pitch (θ), (C) yaw (δ), (D) UAV inclination angle (Ψ), and (E) the relationship between UAV flight direction and wind direction (η_{wind}). In panels (D) and (E), the example case corresponds to $\phi < 0$, $\theta > 0$, and $\delta = 180°$. The blue plane represents the ground horizontal plane, while the red plane represents the UAV's inclined plane. $\vec{N}_{\phi\theta}$ denotes the normal vector perpendicular to the UAV's inclined plane.
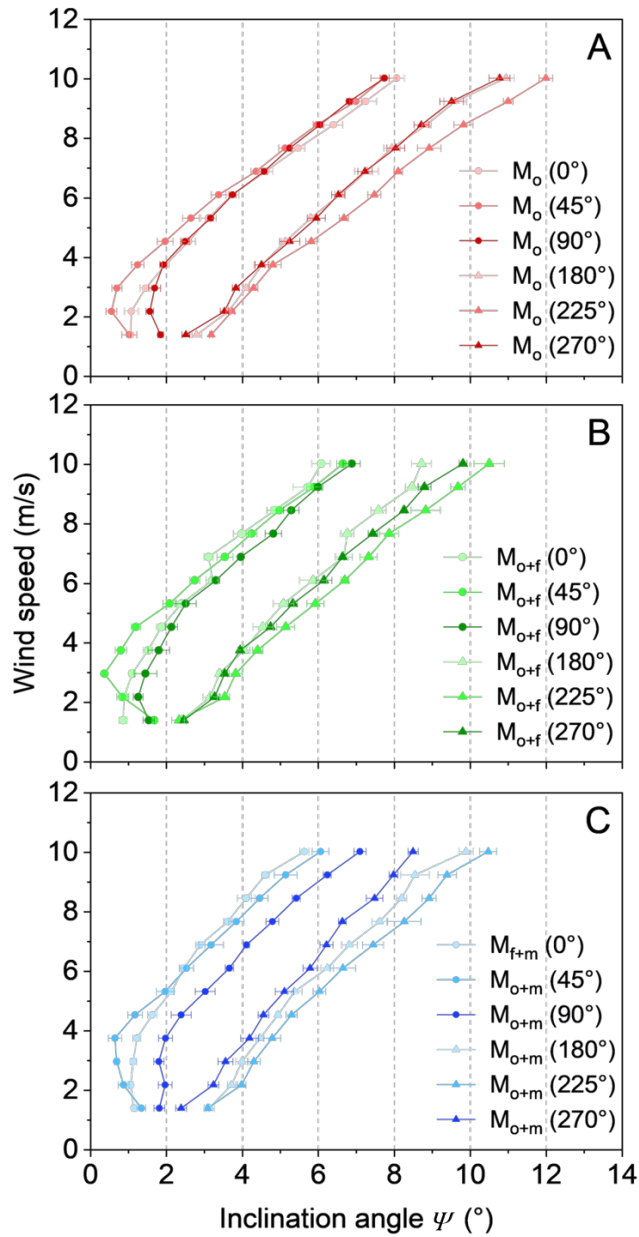
Figure 3 Relationship between UAV inclination angle and wind speed under varying payload (A: default, B: additional front-top payload, C: additional central-top payload) and wind direction (0°, 45°, 90°, 180°, 225°, and 270°) conditions. The payload configurations and relative wind directions are illustrated in Figure 2. The relationships are characterized by power function fits, with coefficients for each flight scenario provided in Table S1.
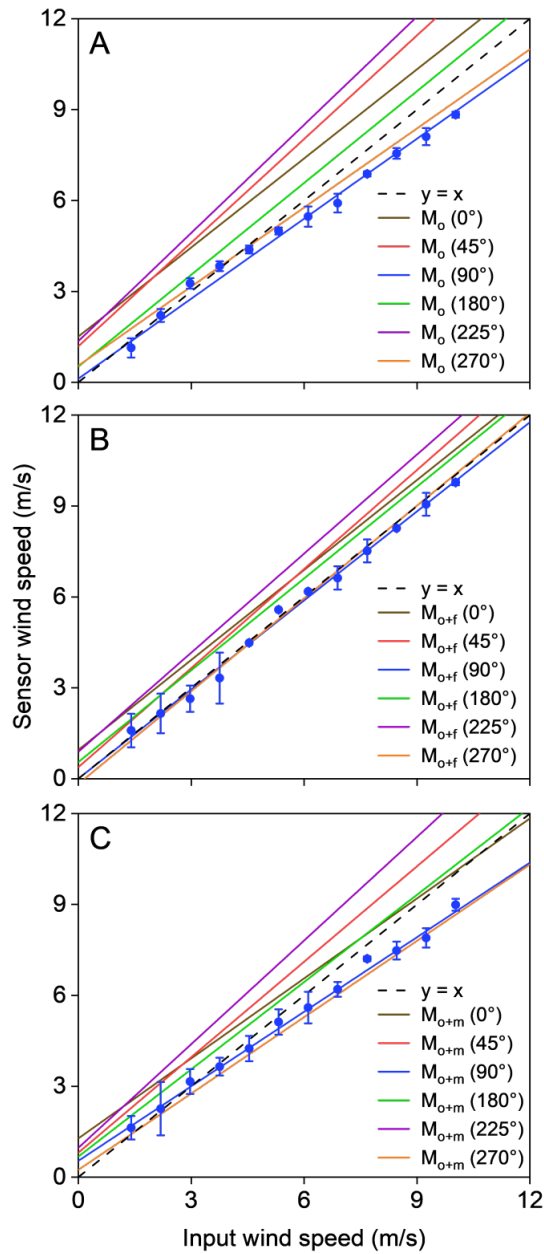
Figure 4 Relationship between input wind speed and sensor-measured wind speed under varying payload (A: default, B: additional front-top payload, C: additional central-top payload) and wind direction (0°, 45°, 90°, 180°, 225°, and 270°) conditions. Both measurements and fitted curves are shown for 90° relative wind direction scenarios, while only fitted curves are presented for other directions. Corresponding fitting parameters are provided in Table S2.
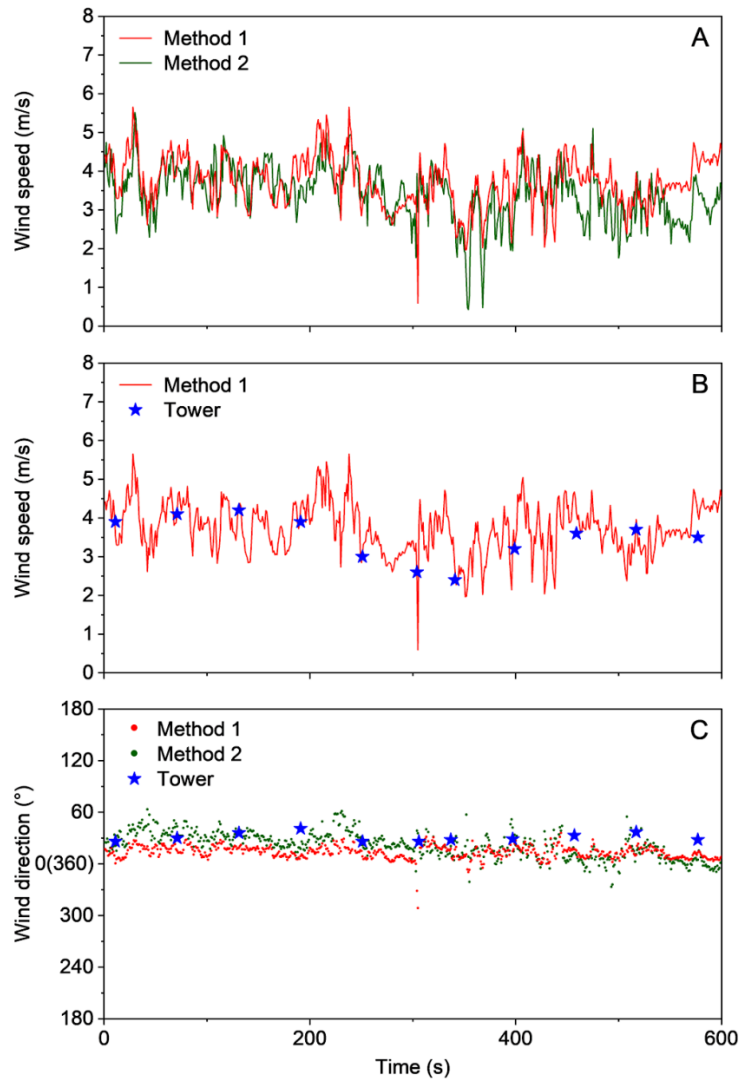
Figure 5 Comparison between UAV-based wind speed estimates (from methods 1 and 2) and reference measurements from the meteorological observation tower during hovering flight operations.
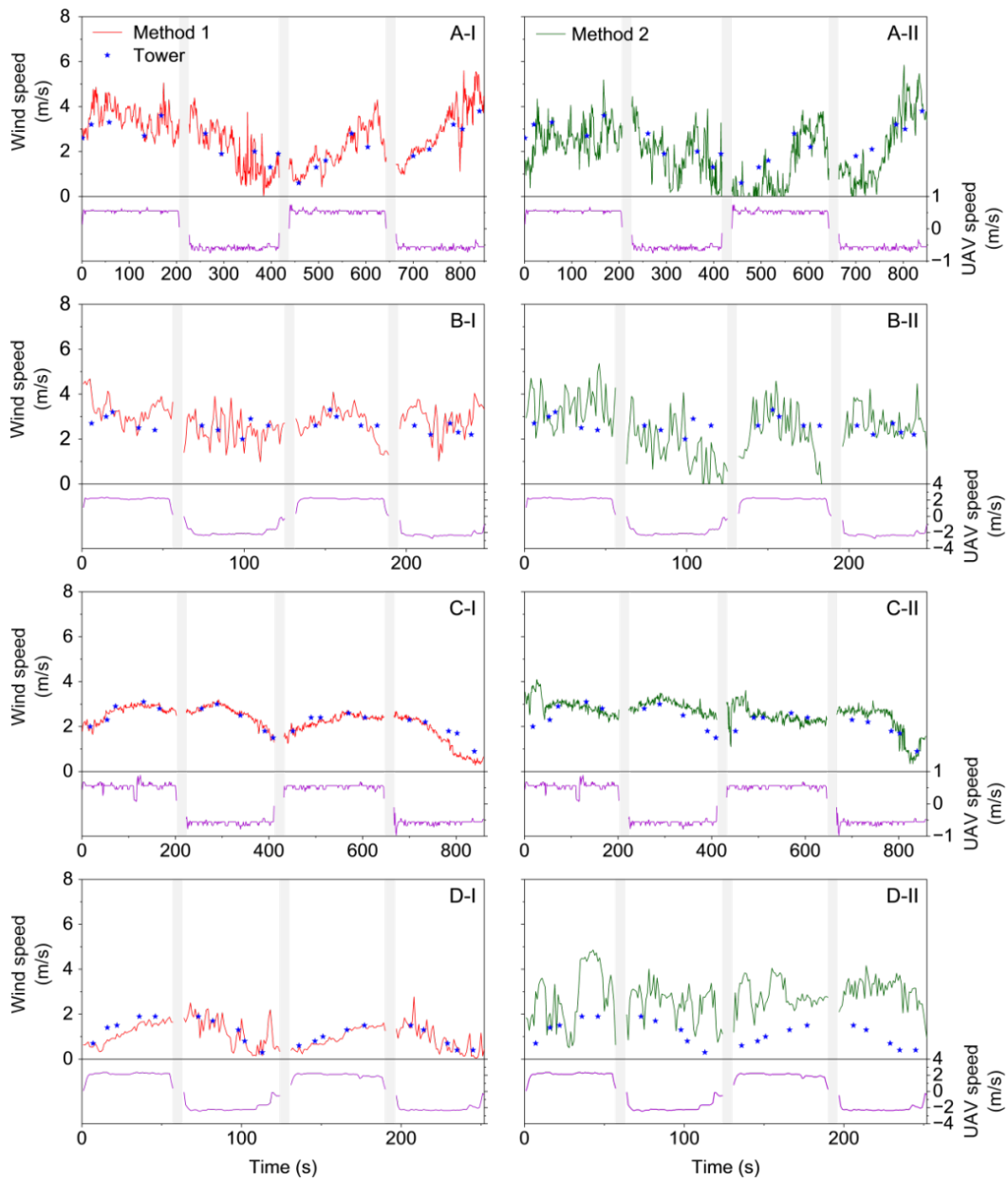
Figure 6 Comparison between UAV-based wind speed estimates and reference measurements from the meteorological observation tower during vertical flight operations: ascending and descending at 0.5 m/s (A) and 2 m/s (B) with default payload, and at 0.5 m/s (C) and 2 m/s (D) with additional front-top payload. Gray shaded areas indicate hovering periods.
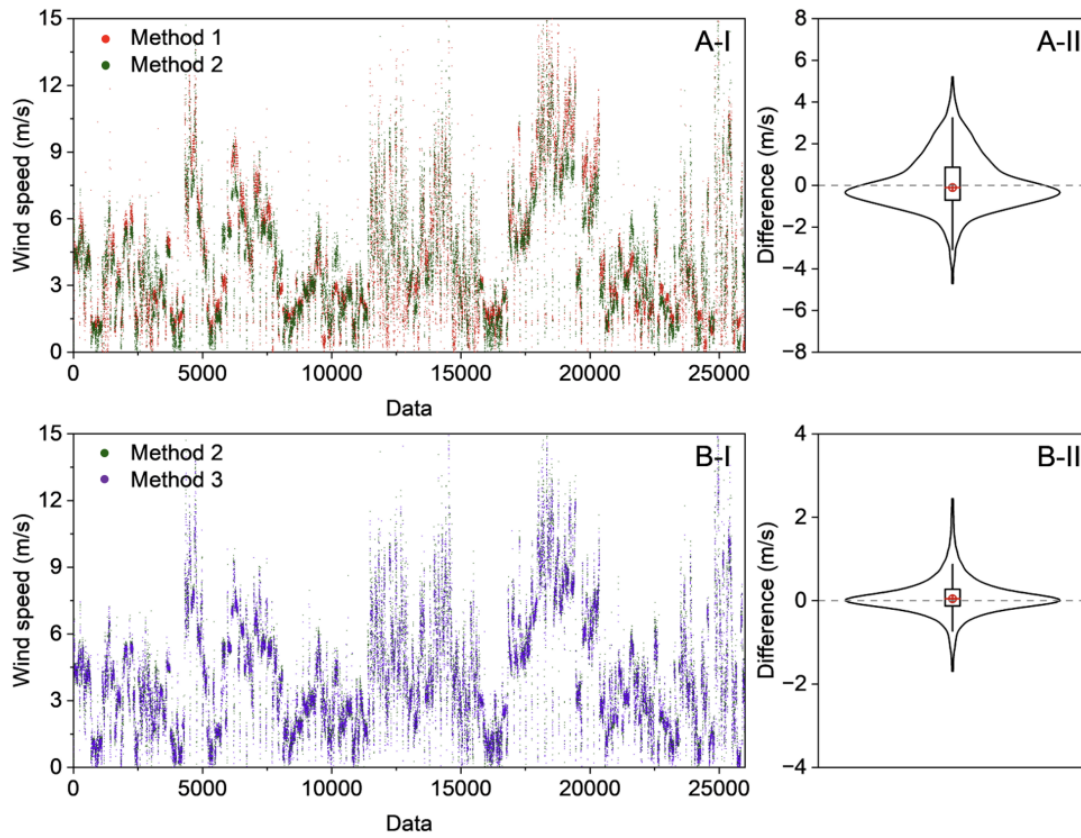
Figure 7 UAV-based wind speed estimation and deviation analysis comparing methods 1 versus 2 (A-I, A-II) and methods 2 versus 3 (B-I, B-II) from the field observation campaign.
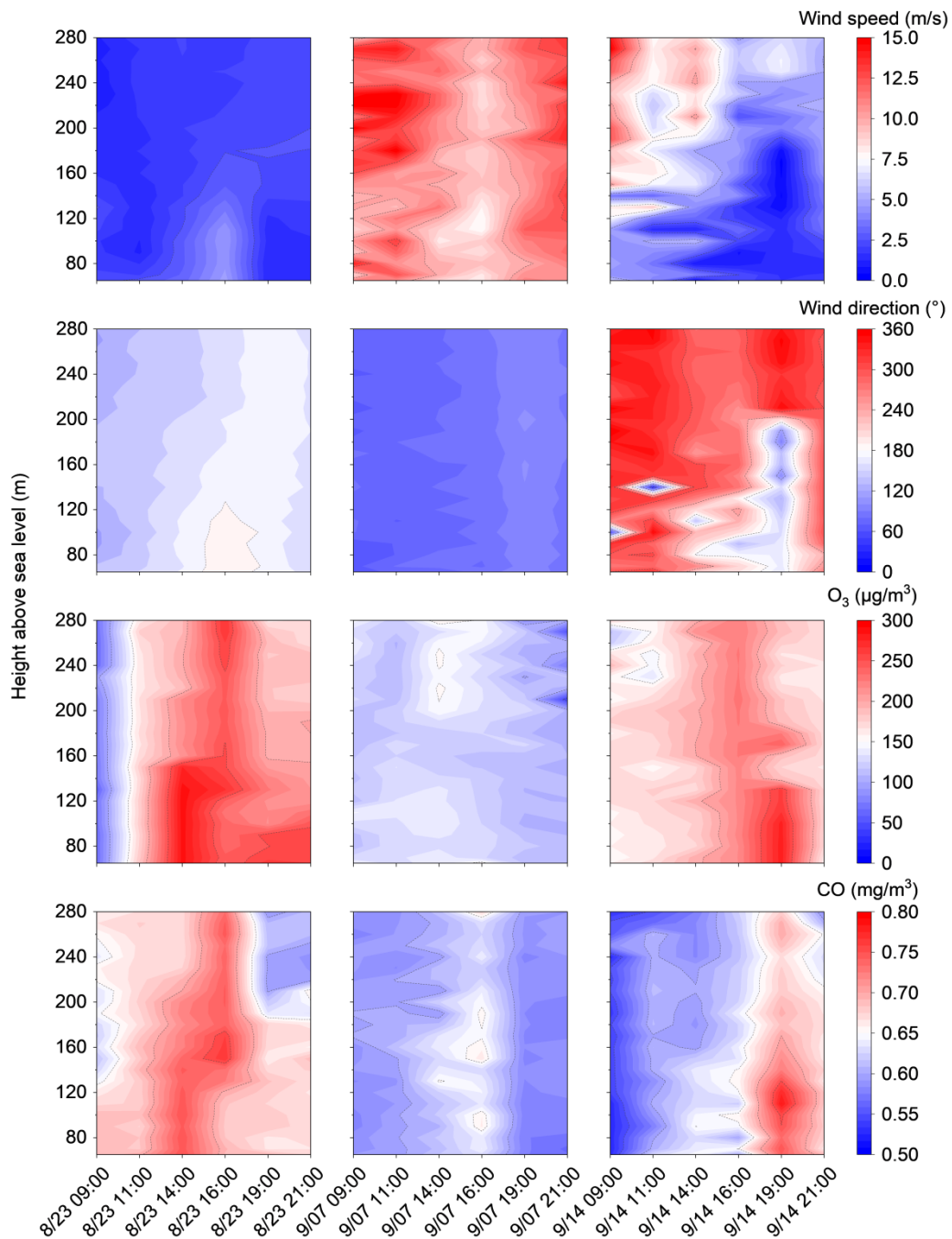
Figure 8   2-D contour plots of the vertical profiles of wind speed, wind direction, O_3 and CO concentrations measured on August 23, September 7, and September 14 of 2022, respectively. All data represent 10-s averages.